Petroleum Science 23 (2026) 913–927

Contents lists available at ScienceDirect

Petroleum Science

journal homepage: www.keaipublishing.com/en/journals/petroleum-science

Original Paper

Stability mechanism and steady-state flow characteristics of oil-resistant foam in high-salinity reservoirs

Lin Sun [a,b,*], Jia-Qi Yin [a], Hong-Ying Sun [c], Yan-Ping Wu [d], Wan-Fen Pu [a], Bing Wei [a,**]

[a] State Key Laboratory of Oil and Gas Reservoir Geology and Exploitation, Southwest Petroleum University, Chengdu, 610500, Sichuan, China
[b] Tianfu Yongxing Laboratory, Chengdu, 610213, Sichuan, China
[c] No. 9 Oil Production Plant, PetroChina Changqing Oilfield Company, Yinchuan, 750006, Gansu, China
[d] Zhuangxi Oil Production Plant of Shengli Oilfield Company, Dongying, 257237, Shandong, China

ARTICLE INFO

Article history:
Received 12 November 2024
Received in revised form
5 November 2025
Accepted 5 November 2025
Available online 10 November 2025

Edited by Yan-Hua Sun

Keywords:
High-salinity reservoirs
Oil-resistant foam
Pseudoemulsion film stability
Dilatational viscoelasticity
In-situ emulsion
Steady-state flow

ABSTRACT

High salinity and high oil content present major challenges to the effectiveness of foam in enhanced oil recovery (EOR). This study introduces RCS, a novel oil-resistant foam system designed for reservoirs with salinity levels reaching 2.1×10^5 mg/L. RCS forms stable foams at oil–water ratios up to 60% and is effective across a wide crude oil viscosity range (10.8–7890 mPa·s). We investigated the film properties of oil-containing foam and the co-permeation behavior of the crude oil–N_2–foam system to elucidate the mechanisms underlying foam stability and steady-state flow. RCS emulsified high-viscosity crude oil into stable, large droplets that accumulated within the plateau borders, reducing drainage. Even at concentrations as low as 0.01 wt%, RCS formed stable pseudoemulsion films that prevented intrusion into the gas–water interface, allowing the foam half-life to be mainly controlled by the dilatational viscoelasticity of the interface. With increasing oil–water ratios, both drainage resistance and dilatational modulus increased, extending the drainage and foam half-lives. Coreflood experiments showed that co-injection of RCS with N_2 and crude oil produced stable foams and in-situ emulsions. At 5% oil fractional flow, the critical foam quality (f_g^*) remained unchanged compared to oil-free conditions, although the maximum apparent viscosity decreased by 29.8%. At 10% oil fractional flow, f_g^* shifted to a lower value, while the apparent viscosity in the low-quality regime increased markedly—exceeding that of the oil-free condition. These findings highlight that while crude oil more strongly impairs foam stability in porous media than in bulk, the formation of in-situ emulsions can partially offset or even enhance mobility control through a synergistic Jamin effect. Therefore, in-situ emulsification should be emphasized in foam applications within oil-containing environments.

1. Introduction

The escalating global energy demand has significantly intensified research into enhanced oil recovery (EOR) over the past few decades (Talebian et al., 2014; Liang et al., 2019; Hassan et al., 2020). Among the various EOR methods, gas injection is particularly notable for its effectiveness and widespread application (Stein et al., 1992; Jamaloei and Kharrat, 2012; Wei et al., 2018; Guo et al., 2022). However, the inherently low density and viscosity of gas often lead to challenges such as viscous fingering, gravity override, and early gas breakthrough, which compromise gas sweep efficiency. Consequently, there has been a growing interest in the application of foam to mitigate these undesirable phenomena (Yan et al., 2006; Ma et al., 2012; Sun et al., 2016). Stable foams can reduce gas mobility and divert gas toward lower permeability regions, thereby expanding the gas sweep area and enhancing oil recovery.

Foam stability in reservoir environments is influenced by numerous factors, with salinity being among the most critical (Sun et al., 2019; Harati et al., 2020; Roncoroni et al., 2021; Tang et al., 2023). While low salinity tends to stabilize foam, high salinity typically has a detrimental impact on foam stability. For instance, Majeed et al. (2020) observed a remarkable decrease in

* Corresponding author.
** Corresponding author.
E-mail addresses: slswpu@swpu.edu.cn (L. Sun), bwei@swpu.edu.cn (B. Wei).
Peer review under the responsibility of China University of Petroleum (Beijing).

https://doi.org/10.1016/j.petsci.2025.11.014

the stability of sodium alpha-olefin sulfonate (AOS) foam at a NaCl concentration of 1 mol/L. They noted that excess electrolytes surrounded AOS molecules, preventing them from entering the micelle structure that constituted the foam film, thereby reducing film stability. Similarly, He et al. (2022) reported that the stability of sodium dodecyl benzene sulfonate (SDBS) foam weakened at a salinity of 160,599 mg/L due to the formation of insoluble salts between Ca^{2+}/Mg^{2+} ions and SDBS anions, leading to decreased surface activity of the SDBS solution. Recent research has revealed that betaine foams can withstand salinities up to 2×10^5 mg/L and exhibit enhanced foam stability with increasing salinity (Sun et al., 2022, 2023). Our previous work demonstrated that as salinity increased, more betaine surfactant molecules adsorbed onto the gas–water interface with a lower diffusion rate, leading to an increase in dilatational modulus, thereby improving foam stability.

Crude oil also plays a crucial role in affecting foam stability. Researchers have introduced parameters such as the entry coefficient (E), spreading coefficient (S), and bridging coefficient (B) to assess foam stability in the presence of oil (Harkins and Feldman, 1922; Garrett, 1980; Aveyard et al., 1994), as detailed in Eqs. (1)–(3).

$$E = \sigma_{w/g} + \sigma_{w/o} + \sigma_{o/g} \tag{1}$$

$$S = \sigma_{w/g} - \sigma_{w/o} - \sigma_{o/g} \tag{2}$$

$$B = \sigma_{w/g}^2 + \sigma_{w/o}^2 - \sigma_{o/g}^2 \tag{3}$$

where $\sigma_{w/g}$ is the surface tension between the surfactant solution and gas; $\sigma_{w/o}$ is the interfacial tension between oil and the surfactant solution; and $\sigma_{o/g}$ is the surface tension between oil and gas.

When E is negative, the corresponding S and B are also negative, indicating that foam can remain stable in the presence of oil (Babamahmoudi and Riahi, 2018). Conversely, when E and S are positive, oil will enter the surface of the foam film and spread, thinning the film and accelerating foam rupture (Harkins, 1941). If spreading does not occur ($S < 0$), oil droplets accumulate at the gas–water interface, gradually increasing in size. When oil droplets become large enough to form an unstable oil bridge across the foam film ($B > 0$), the film is prone to rupture (Garrett, 1980). However, these coefficients characterize oil–foam interaction based solely on interfacial and surface tensions, which introduces significant limitations and does not always accurately predict the stability of oil-containing foam.

The prevailing viewpoint holds that the stability of oil-containing foam is closely related to the state of crude oil within the foam film. Crude oil, upon interacting with foam, can either solubilize in surfactant micelles, forming solubilized oil, or distribute as emulsified oil droplets within the foam film (Koczo et al., 1992). Solubilized oil can adversely affect foam stability by reducing the repulsive force between micelles and diminishing their effective volume, thereby accelerating film thinning (Lee et al., 2014). The influence of emulsified oil droplets on foam stability depends on the stability of the pseudoemulsion film formed by crude oil and the gas–water interface of the foam film. Stable pseudoemulsion films are beneficial for foam stabilization (Pu et al., 2019), but high salinity always destabilizes the pseudoemulsion film. Pu et al. (2017) found that heavy oil with 20% oil content significantly improved the foam composite index at salinity levels below 8.8×10^4 mg/L, whereas it disrupted the foam at higher salinity levels. Vikingstad et al. (2005) reported that when the crude oil concentration was 5 wt%, stable AOS foam was produced at a 1 wt% NaCl concentration, but no foam formed when the NaCl concentration was raised to 5 wt%. Rohani et al. (2014) elucidated that in high-salinity environments, the reduction in electrostatic repulsion within the pseudoemulsion film facilitated the entry of oil droplets into the foam film. Consequently, in reservoirs with both high salinity and high oil content, foam stability faces significant challenges. Moreover, there is no reliable quantitative method for in-situ evaluation of pseudoemulsion film stability. Most studies rely on qualitative microscopic observations or indirectly assess through the interfacial properties of gas–water or oil–water systems (Wei et al., 2020; Lai et al., 2021). This limited understanding often results in foam exhibiting insufficient oil resistance in field applications.

The stability of bulk foam is positively correlated with its mobility control capability in porous media, while steady-state flow behavior offers a more direct approach for characterizing foam flow resistance and optimizing injection strategies, thereby maximizing the economic benefits of foam EOR processes. In oil-free porous media, steady-state foam flow exhibits two distinct regimes: low-quality and high-quality regimes (Osterloh and Jante, 1992; Kim et al., 2004). In the low-quality regime, the pressure gradient is independent of the apparent liquid velocity, with foam behavior controlled by gas trapping and mobilization. In the high-quality regime, the pressure gradient is independent of the apparent gas velocity, with foam behavior governed by bubble coalescence at the critical capillary pressure (P_c^*). A critical foam quality (f_g^*) exists in the transition regime between low-quality and high-quality regimes, where the foam exhibits the maximum apparent viscosity (Li et al., 2023). In the presence of oil, these two regimes persist, but both are influenced by oil–foam interactions. The extent of gas mobility reduction decreases in the low-quality regime, and the critical water saturation (S_w^*) required for stable foam increases in the high-quality regime, making the foam more susceptible to rupture (Tang et al., 2019a, 2019b). The impact of oil on foam flow resistance varies with oil content, and investigations in this area are primarily conducted at unstable or immobile oil contents, limiting the understanding of foam mobility control in the presence of crude oil (Andrianov et al., 2011; Simjoo and Zitha, 2013; Amirmoshiri et al., 2021).

To address these issues, we developed an oil-resistant and salt-tolerant foam system by introducing an oil-resistant additive into a mixture of an anionic-nonionic surfactant and a betaine surfactant. By examining the macroscopic and microscopic structural evolution of oil-containing foam, pseudoemulsion film stability, and surface dilatational viscoelasticity, we comprehensively investigated the mechanisms by which crude oil affects foam stability under varying oil–water ratios. Additionally, we characterized the steady-state foam flow behavior under various fixed oil contents using multiphase co-injection experiments. The results of this study enhance our understanding of the stability and mobility control capability of foam in the presence of crude oil, contributing to the advancement of foam EOR.

2. Materials and methods

2.1. Materials

The surfactants used in this study were supplied by Yusuo Chemical Technology Co., Ltd. These included fatty alcohol polyoxyethylene ether sulfonate (WR and AT, active content 70%), betaine surfactant (WC and AE, active content 35%), alpha olefin sulfonate (AOS, active content 35%), sodium dodecyl sulfate (SDS, active content 30%), and an oil-resistant additive (OS, fluorocarbon surfactant with an active content of 30%). Petroleum ether (boiling

range 90–120 °C) was purchased from Chron Chemicals Co., Ltd. All chemicals were used as received.

Unless otherwise specified, brine with a NaCl concentration of 9.36×10^4 mg/L was used to prepare surfactant solutions at a total concentration of 0.2 wt%. Dehydrated heavy crude oil (oil A) and light crude oil (oil E) were sampled from an oilfield in western China. The two types of crude oil were mixed in different volume ratios to produce oils B, C, and D with progressively decreasing viscosities, as shown in Table 1. Dry nitrogen gas with a purity of 99.89% was used in all experiments.

Artificial sandstone cores were used for multiphase co-injection experiments. The cores were dried at 150 °C for one day to eliminate any moisture before testing porosity and brine permeability. The petrophysical properties of the cores are presented in Table 2.

2.2. Bulk foam performance evaluations

2.2.1. Foamability and foam stability

Foams were generated using the Waring blender method. Crude oil and a 100 mL surfactant solution were added to a foam generator before measurements. The oil–water ratio, defined as the volume ratio of crude oil to surfactant solution, was varied from 10% to 60%. The total volume of the crude oil and surfactant solution was recorded as the total liquid volume (V_0). The mixture was sheared at 6000 rpm for 1 min to generate the oil-containing foam, which was then transferred to a 1000 mL graduated cylinder to measure the foaming volume (V_{max}). The changes in drained liquid volume (V_l) and foam volume (V_f) were monitored over time. Foam stability was assessed based on the drainage half-life and foam half-life, representing the times required for V_l to reach half of V_0 and for V_f to decrease to half of V_{max}, respectively. Additionally, the liquid volume fraction (f_w) was calculated using Eq. (4) to analyze the decay behavior of the foam. All experiments were conducted in triplicate at ambient temperature (25±2 °C) to ensure reproducibility.

$$f_w = (V_0 - V_l) \Big/ V_f \times 100\% \tag{4}$$

2.2.2. Foam microstructure

A Leica DM2700M metallographic microscope was used to visualize the foam microstructure at room temperature. During the foam decay process, samples of foam were collected at specified time points from the same location in the graduated cylinder using a glass rod and transferred onto a microscope slide for observation. The foam microstructure images were processed using ImageJ software for grayscale conversion and binarization. Measurements of the bubble diameter (d_i) and the number of bubbles (n_i) were taken, and the Sauter mean bubble diameter (D_{32}) was calculated using Eq. (5).

$$D_{32} = \sum \left(n_i d_i^3\right) \Big/ \sum \left(n_i d_i^2\right) \tag{5}$$

Table 1
Crude oil types and viscosities.

Crude oil type	Viscosity at 50 °C, mPa·s	Volume ratio of oil A to oil E
Oil A	7890	1:0
Oil B	900	1:1
Oil C	650	1:1.7
Oil D	260	1:2.2
Oil E	10.8	0:1

2.3. Surface/interfacial behavior measurements

2.3.1. Interfacial tension

The interfacial tension (IFT) was measured using a KRÜSS spinning drop tensiometer (SDT) equipped with an integrated image-capture device and Advance™ software, which automatically calculated the IFT. The rotation rate of the drops was set at 6000 rpm. All IFT measurements were conducted at 25 °C.

2.3.2. Dilatational surface viscoelasticity

The oscillating drop method was employed to assess dilatational viscoelasticity at 25 °C using the KRÜSS drop shape analyzer (DSA100). In a typical experiment, 10 μL of surfactant solution was dripped onto the needle end and left to equilibrate. A sinusoidal oscillation, with a frequency range of 0.02–2 Hz and an amplitude of 10%, was then applied to the droplet. The interfacial area (A) and surface tension (σ) at various frequencies were measured, and the dilatational modulus (E), elastic modulus (E'), and viscous modulus (E'') were calculated according to Eqs. (6)–(8) (Amani et al., 2020). The DSA100 automatically performed these analyses.

$$E = d\sigma / d\ln A \tag{6}$$

$$E' = |E|\cos\theta \tag{7}$$

$$E'' = |E|\sin\theta \tag{8}$$

2.3.3. Surfactant concentration in the aqueous phase of foam film

During foam decay, the aqueous phase drained from the foam is equivalent to that remaining in the foam film. Therefore, the surfactant concentration in the aqueous phase of the foam film can be estimated by measuring the concentration of the drained aqueous phase. Prior to determining the surfactant concentration, the surface tension of the foam system was tested across a surfactant concentration range from 0.002 to 0.2 wt% using the platinum plate method (Wang et al., 2021). The resulting relationship between surface tension and surfactant concentration is depicted in Fig. 1. Based on this curve, the critical micelle concentrations (CMC) of RC (The mass ratio of surfactants WR to WC is 3:1) and RCS (The mass ratio of mixed surfactants RC to OS is 7:3) were determined to be 0.022 and 0.015 wt%, respectively. That is, the surfactant concentration used for bulk foam tests was approximately an order of magnitude higher than the CMC.

After the oil-containing foam in the bulk foam test reached its half-life, the drained liquid was collected and centrifuged to facilitate oil–water separation. The aqueous phase was extracted using a separatory funnel, then diluted tenfold with brine to ensure the surfactant concentration was below the CMC. The surface tension of the diluted aqueous phase was measured, and the surfactant concentration was determined based on the surface tension-surfactant concentration relationship depicted in Fig. 1. The concentration was then multiplied by ten to derive the surfactant concentration in the foam film's aqueous phase.

2.3.4. Pseudoemulsion film stability

The stability of the pseudoemulsion film was evaluated using a custom-built apparatus, designed according to the drop and bubble micro manipulator (DBMM) principle (Won et al., 2014; Ahmadi et al., 2023), as depicted in Fig. 2. The primary component of the setup was an organic glass cylinder, with a diameter of 1.5 cm. The cylinder was pre-filled with the surfactant solution, forming a meniscus approximately 0.2 cm above the horizontal

Table 2
Petrophysical properties of cores.

Core number	Length, mm	Width, mm	Height, mm	Porosity, %	Brine permeability, mD
#1	301.0	44.2	44.9	18.8	460.0
#2	302.0	44.5	45.0	17.8	502.0

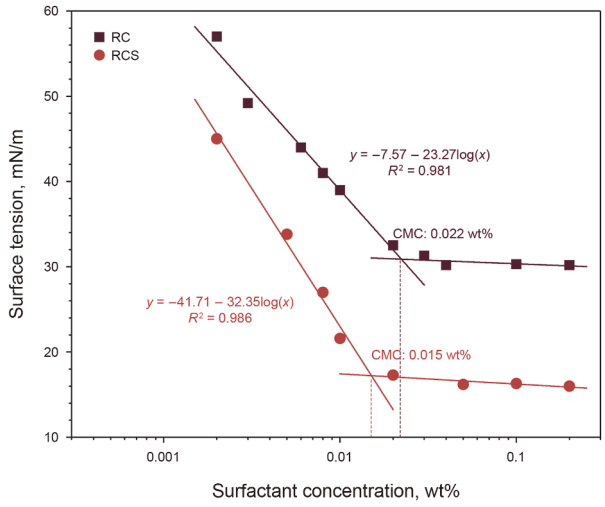

Fig. 1. Relationship between surfactant concentration and surface tension for foam systems RC and RCS.

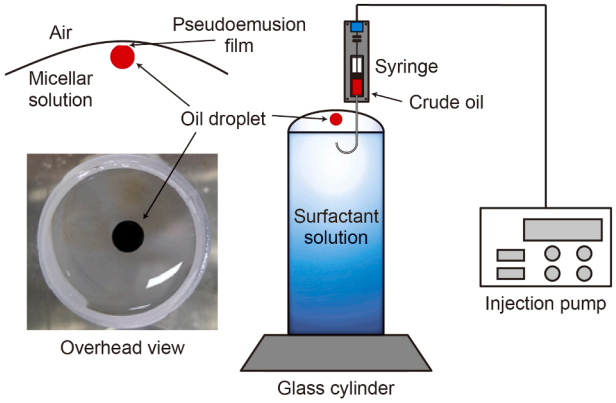

Fig. 2. Schematic of the device used to determine pseudoemulsion film stability.

plane. At the beginning of the experiment, a 10 μL oil droplet was introduced beneath the gas–water interface using a syringe equipped with a U-shaped needle. The pseudoemulsion film formed as the oil droplet approached the gas–water interface. A camera positioned directly above the cylinder recorded the time required for the oil droplet to spread on the gas–water interface. Each sample was measured three times, and the average time was used as the final result to assess the stability of the pseudoemulsion film.

Each test in Sections 2.2 and 2.3 was performed in triplicate to ensure reproducibility and minimize random error.

2.4. Multiphase co-injection measurements

The multiphase co-injection experiment was performed using a high-temperature, high-pressure (HTHP) core-flooding system, as shown in Fig. 3. The core holder was fitted with four pressure transducers to monitor the pressure drop in each section along the core. The surfactant solution, N_2, and crude oil were each loaded into separate piston containers, with injection rates controlled by three duplex pumps and a gas mass-flow controller. The reservoir temperature and back pressure were maintained at 90 °C and 15.0 MPa, respectively.

The crude oil–N_2–foam system co-injection experiments were conducted by incrementally increasing the oil fractional flow (f_o), with the foam quality (f_g) randomly selected from the values listed in Table 3. The values of f_o and f_g were calculated using Eqs. (9) and (10), respectively.

$$f_o = q_o \Big/ \left(q_o + q_g + q_l\right) \tag{9}$$

$$f_g = q_g \Big/ \left(q_g + q_l\right) \tag{10}$$

where q_o, q_g, and q_l are the injection flow rates of crude oil, N_2, and surfactant solution, respectively.

The total injection rate (Q) was fixed at 0.700 mL/min, corresponding to a superficial velocity of 2.70 m/d. When the pressure drop in the middle section (ΔP_2) stabilized with acceptable fluctuation, it indicated a steady flow state, signifying that foam generation and collapse had reached dynamic equilibrium. The equilibrium value of ΔP_2 was recorded and used to calculate the apparent viscosity (μ) using Eq. (11). Following each test, the core was sequentially cleaned with petroleum ether, N_2, and brine.

$$\mu = kA\Delta P_2 / QL_2 \tag{11}$$

where k is the brine permeability; A is the cross-sectional area; and L_2 is the length of the middle core section.

Prior to conducting the three-phase co-injection experiments, the foam system and N_2 were co-injected at various foam qualities to characterize the steady-state flow behavior of foam in the absence of crude oil. Additionally, co-injection of the foam system with crude oil was performed to determine the steady-state flow resistance of the in-situ emulsion. Cores #1 and #2 were used to perform the multiphase co-injection experiments with RC and RCS, respectively, ensuring consistency in experimental conditions.

3. Results and discussion

3.1. Development of an oil-resistant and salt-tolerant foam system

3.1.1. Screening of foaming agent

Four salt-tolerant surfactants and two conventional surfactants were selected for bulk foam tests at a 10% oil–water ratio. As shown in Fig. 4(a), all surfactants effectively generated foam in the presence of crude oil A. Among these, the fatty alcohol polyoxyethylene ether sulfonate salts, WR and WC, demonstrated superior foamability and foam stability, respectively. Based on this, WR and WC were blended at a 3:1 mass ratio to form the RC foam system. This combination produced a clear synergistic effect: the foaming volume of RC increased by 18.7% compared to WR, while its drainage and foam half-lifves were 5.7 and 1.2 times those of WC, respectively. Fig. 4(b) presents the liquid volume fraction (f_w) of

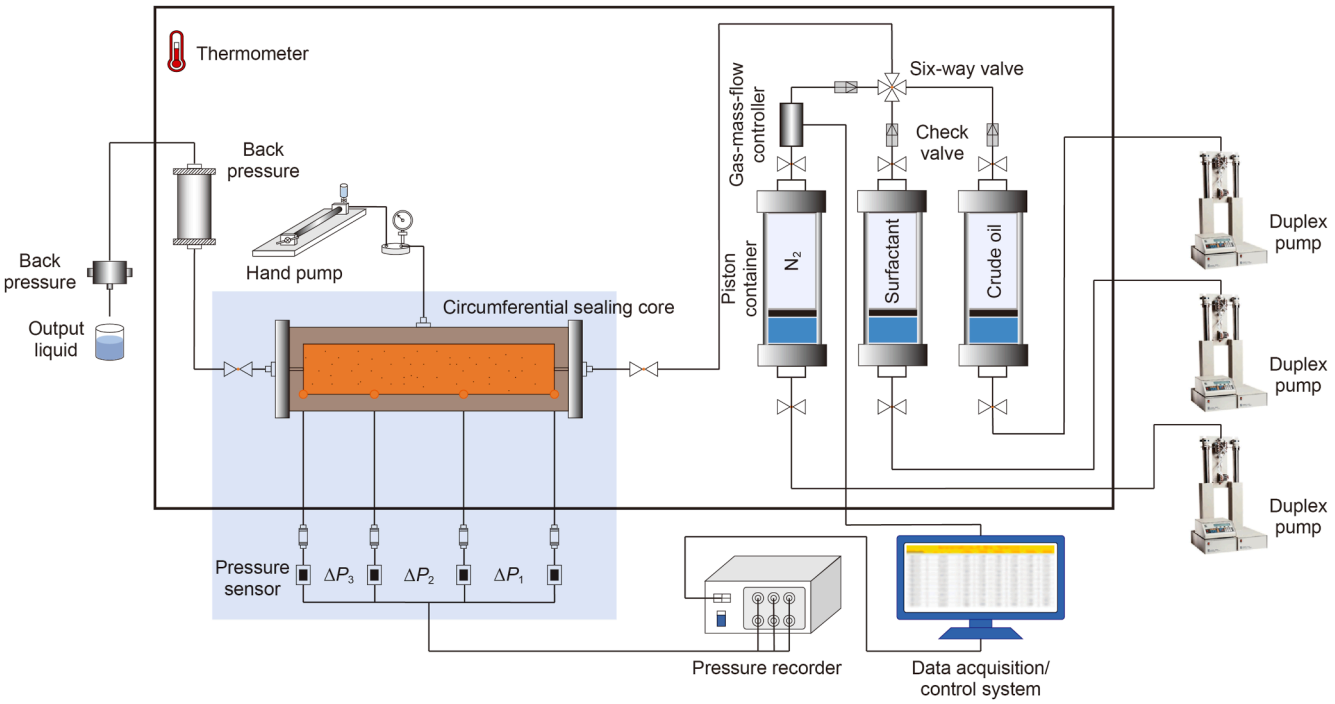

Fig. 3. Schematic of the experimental setup for multiphase co-injection experiments.

Table 3
Injection flow rates and oil–water ratios for each phase under different foam qualities and oil fractional flows.

Oil fractional flow, %	Foam quality, %	Oil flow rate, mL/min	Surfactant flow rate, mL/min	N_2 flow rate, mL/min	Oil–water ratio, %
0	0	0	0.700	0	0
	20		0.560	0.140	
	40		0.420	0.280	
	60		0.280	0.420	
	80		0.140	0.560	
	90		0.070	0.630	
	95		0.035	0.665	
5	0	0.035	0.665	0	5.3
	20		0.532	0.133	6.6
	40		0.399	0.266	8.8
	60		0.266	0.399	13.2
	80		0.133	0.532	26.3
	90		0.067	0.598	52.2
10	0	0.070	0.630	0	11.1
	20		0.504	0.126	13.9
	40		0.378	0.252	18.5
	60		0.252	0.378	27.8
	80		0.126	0.504	55.6

oil-containing foams during their half-lives. Initially, f_w declined rapidly due to gravity- and capillarity-driven drainage. Since all f_w values dropped below 36% within 5 min, we refer to all gas–liquid mixtures as "foam" for consistency. Upon reaching a critical point, f_w either stabilized or showed a slight increase, marking the transition where coarsening and coalescence became dominant in foam decay (Mensire and Lorenceau, 2017). The f_w curve for RC oil-containing foam exhibited the smallest slope and the longest plateau, indicating the slowest drainage and highest film stability.

To determine the resistance of RC foam to different crude oils, 0.2 wt% RC solution was mixed with oils of varying viscosities at a fixed 20% oil–water ratio. As shown in Fig. 5(a), the foaming volume, drainage half-life, and foam half-life of RC oil-containing foam all increase with increasing crude oil viscosity. For oils with viscosities ranging from 650 to 7890 mPa·s, the drainage half-life exceeded that of the oil-free foam, reaching up to twice its value. However, low-viscosity oils significantly impaired foam performance. For instance, in the presence of crude oil with a viscosity of 10.8 mPa·s, the foaming volume and foam half-life decreased by 51% and 98%, respectively. The steady stage of its f_w curve was completely absent (Fig. 5(b)), highlighting the limited resistance of the RC foam film to such oils and the need for further enhancement.

3.1.2. Enhancing oil resistance

To improve the RC foam stability under oil-containing conditions, an oil-resistant additive (OS) was incorporated at concentrations ranging from 0.02 to 0.10 wt%. Crude oil C was used at a 10% oil–water ratio to identify the optimal mixing ratio of RC and OS.

Fig. 6 demonstrates that the introduction of OS significantly enhanced the tolerance of RC to crude oil C, particularly by

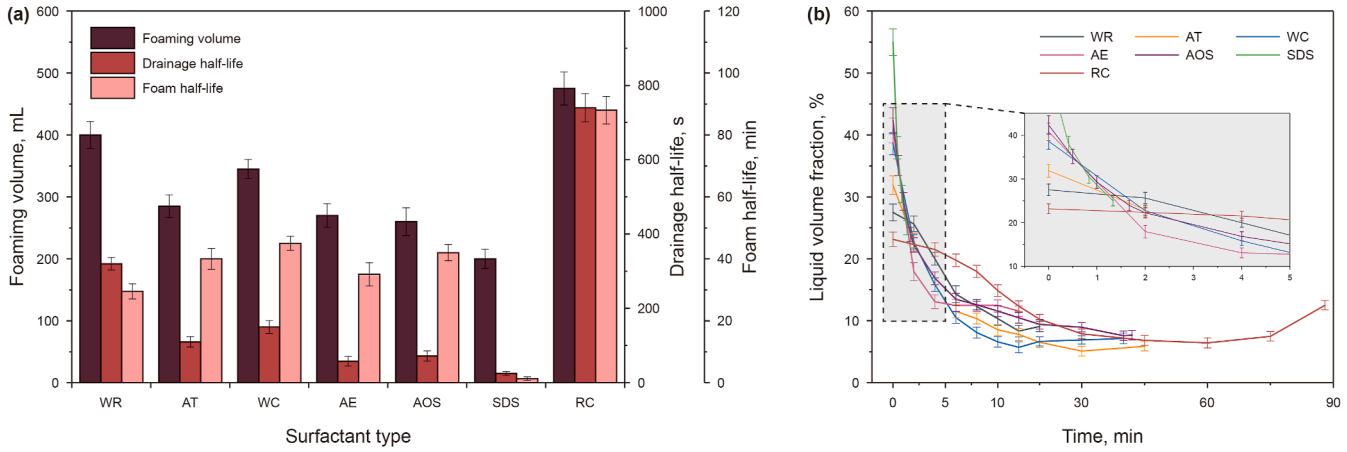

Fig. 4. (**a**) Properties of oil-containing foams formed by different foam systems. (**b**) Liquid volume fraction curves during the foam half-life. Crude oil A was used as the oil phase, the foam system concentration was 0.2 wt%, and the oil–water ratio was 10%.

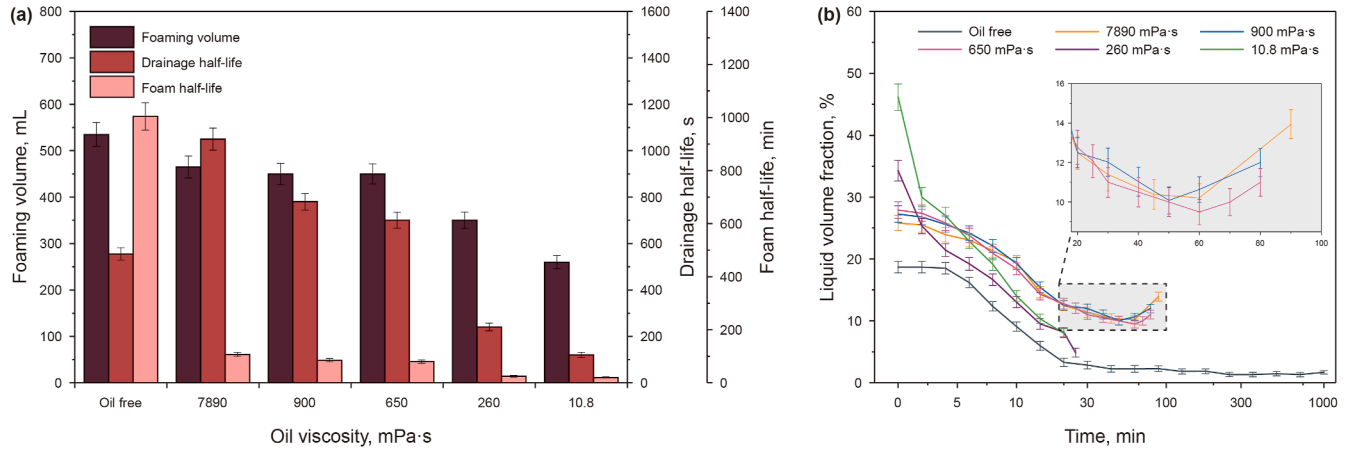

Fig. 5. (**a**) Properties of oil-containing foams formed by RC and crude oils with different viscosities. (**b**) Liquid volume fraction curves during the foam half-life. The RC concentration was 0.2 wt% and the oil–water ratio was 20%.

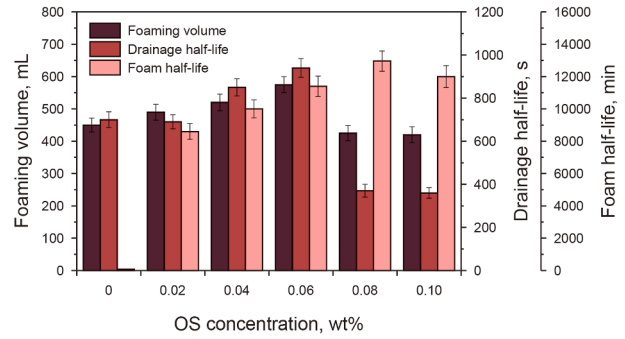

Fig. 6. Properties of oil-containing foams formed by RC and OS with different concentrations. Crude oil C was used as the oil phase, the foam system concentration was 0.2 wt%, and the oil–water ratio was 10%.

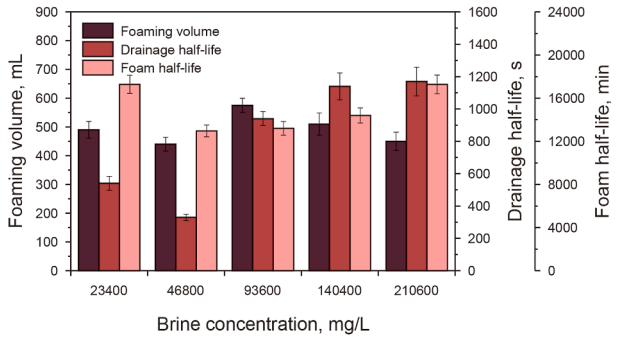

Fig. 7. Properties of RCS oil-containing foams under varying NaCl concentrations. Crude oil C was used as the oil phase, the foam system concentration was 0.2 wt%, and the oil–water ratio was 10%.

extending the foam half-life. Even at a concentration as low as 0.02 wt%, OS increased the foam half-life by more than a hundredfold. As the OS concentration increased, the properties of the oil-containing foam initially improved and then declined. The foam half-life was maximized at an OS concentration of 0.08 wt%, while the foaming volume and drainage half-life were optimized at 0.06 wt%. Balancing performance and cost, RC and OS were blended at a 7:3 ratio to form the RCS system.

To evaluate the applicability of RCS foam in high-salinity reservoirs, its performance was further tested under varying salinities. As shown in Fig. 7, RCS produced stable oil-containing foam across a wide salinity range, from 2.34×10^4 to 2.106×10^5 mg/L, with minimal fluctuation (30.7%) in foaming volume. Notably, as

salinity increased from 4.68 × 10^4 to 2.106 × 10^5 mg/L, both drainage and foam half-lives increased unexpectedly. The foam exhibited its strongest stability at the highest tested salinity, underscoring its distinct advantage in high-salinity conditions.

Further tests examined RCS foam stability with crude oils of various viscosities and contents. While foamability declined in the presence of oil, RCS consistently maintained excellent foam stability (Fig. 8). Compared to RC, RCS offered a more than 68-fold increase in foam half-life under identical oil conditions. Interestingly, the resistance of the RCS foam film to crude oil increased as crude oil viscosity decreased—opposite to the trend observed with RC foam film. When the oil viscosity was ≤ 650 mPa·s, the foam half-life of RCS surpassed that of the oil-free foam, peaking at 10.8 mPa·s with a value 1.86 times greater than the oil-free counterpart.

Fig. 9 demonstrates that the response of RCS foam stability to increasing oil–water ratio also differs significantly from that of RC foam stability. In the presence of crude oil C, the drainage half-life of RC foam peaked at an oil–water ratio of 40%, while its foam half-life decreased dramatically as the oil content increased. At just 10% oil–water ratio, the foam half-life of RC foam dropped by 92% compared to its oil-free counterpart. In contrast, both the drainage and foam half-lives of RCS foam increased with the oil–water ratio. At a 60% oil–water ratio, the drainage and foam half-lives of RCS foam increased to 5.5 and 1.3 times those of the oil-free case, respectively. A similar trend was observed with low-viscosity oil E, where the foam half-life increased with oil content and reached 2.4 times the oil-free value at a 60% oil–water ratio.

These results demonstrate that the incorporation of OS significantly improves the oil resistance of RC foam, enabling stable foam formation and performance across a wide range of oil-bearing and high-salinity conditions.

3.2. Mechanisms of crude oil impact on foam stability

3.2.1. Mechanisms affecting drainage half-life

The bulk foam drainage is primarily governed by the coupling between the bulk liquid flow within the films, plateau borders, and nodes, and the surface flow in the surfactant monolayers (Etemad et al., 2020; Ritacco, 2024; Moradpour et al., 2024). Crude oil influences drainage half-life through two main mechanisms. First, dispersed oil droplets obstruct drainage channels, slowing drainage. The degree of this obstruction depends on factors such as droplet size, quantity, and stability (Telmadarreie and Trivedi, 2018). Second, crude oil reduces surfactant concentration at the gas–liquid interface by drawing surfactant molecules toward the oil–water interface or into the oil phase, accelerating drainage (Farajzadeh et al., 2012). These two conflicting effects lead to inconsistent drainage half-life responses across different foam systems, particularly under varying oil contents and viscosities.

Taking RC foam with oil C as an example, oil droplets were observed to move along with the aqueous phase during drainage. Due to the constraints of drainage channels and the differences in

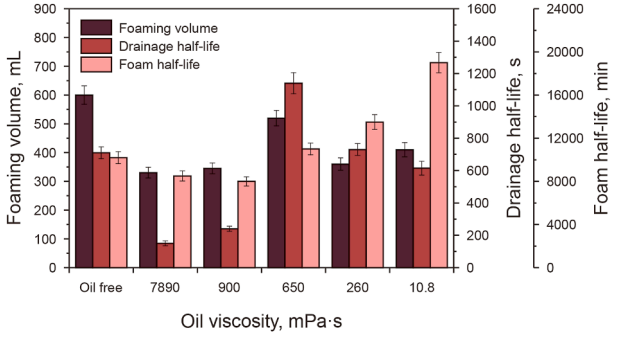

Fig. 8. Properties of oil-containing foams formed by RCS and crude oils with different viscosities. The RCS concentration was 0.2 wt% and the oil–water ratio was 20%.

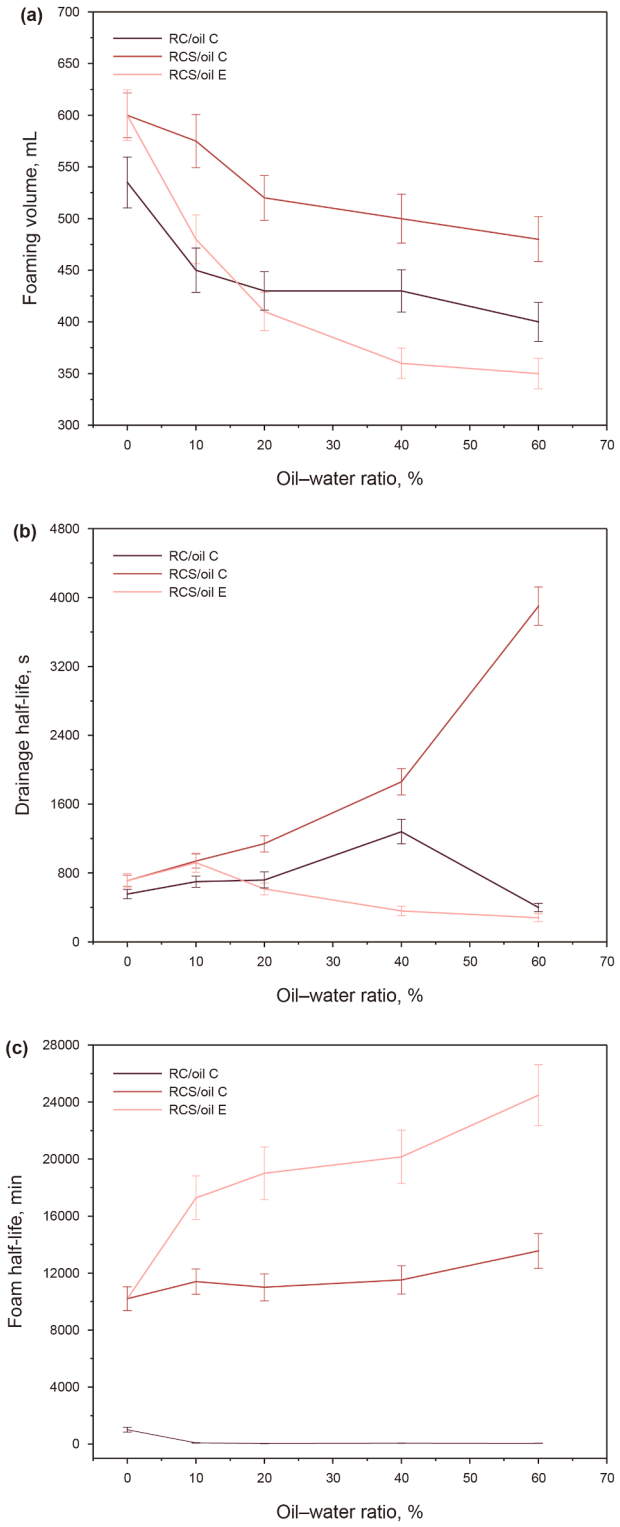

Fig. 9. Effect of oil–water ratio on the properties of oil-containing foams: (**a**) foaming volume, (**b**) drainage half-life, and (**c**) foam half-life. Crude oils C and E were used as oil phases and the foam system concentration was 0.2 wt%.

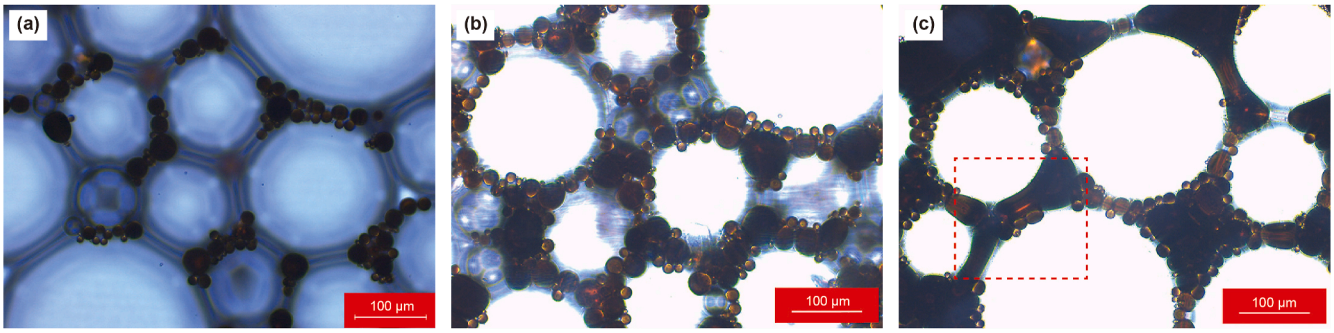

Fig. 10. Microstructure of RC foam after 5 min of foaming in the presence of oil C. The RC concentration was 0.2 wt%, with corresponding oil–water ratios of 10% (**a**), 40% (**b**), and 60% (**c**), respectively.

density and viscosity between oil and water, oil droplets drained more slowly, accumulating in the plateau borders. As the oil–water ratio increased from 10% to 40%, the number of oil droplets within the plateau borders increased significantly. These droplets, remaining stably dispersed, narrowed the drainage channel (Fig. 10(a) and (b)). This accumulation also thickened the plateau borders, thereby reducing the pressure differential between the plateau borders and the film. As a result, the drainage driving force weakened, and the drainage rate further decreased (Vikingstad et al., 2005). However, at a 60% oil–water ratio, the oil–water interfacial area became too large to be tightly packed by RC molecules, leading to the coalescence of oil droplets and the formation of a continuous oil phase within the film, as illustrated in Fig. 10(c). The continuous phase drained rapidly with the aqueous phase, causing a sharp decline in the drainage half-life. In contrast, oil droplets within RCS foam film remained stable even at a 60% oil–water ratio, continuing to hinder drainage. Thus, the drainage half-life of RCS foam with oil C continuously increased as the oil–water ratio gradually increased to 60%.

Fig. 11 shows that oil droplet size within the drainage channels of RCS foam decreased with decreasing oil viscosity. For oil C, the diameter of droplets primarily ranged from 30 to 50 μm, while for oil E, they were mostly under 10 μm. Smaller droplets created less resistance and drained more easily with the aqueous phase. This is supported by Figs. S1 and S2, which show significantly higher oil E content in the drained liquid compared to oil C. As the oil–water ratio increased, the proportion of oil E in the drainage liquid also rose, indicating that smaller droplets exited faster. This explains the continuous decrease in drainage half-life beyond a 10% oil–water ratio when using oil E.

3.2.2. Mechanisms affecting foam half-life

3.2.2.1. Effect of crude oil on foam microstructure evolution. For stable oil-containing foams, the foam half-life is substantially longer than the drainage half-life, indicating that coarsening and coalescence play a more dominant role than drainage in determining foam longevity. Figs. 12 and S3 illustrate the microstructure evolution of oil-containing foams formed by RCS with oils C and E. In oil-free conditions, bubble shapes gradually transitioned from circular to polygonal. However, in the presence of crude oil, particularly at high oil content, bubbles retained a circular shape during decay. With increasing oil–water ratio, oil droplets accumulated in the spaces between bubbles, increasing the distance between them. This inhibited gas diffusion, slowed bubble growth (as shown in Fig. 13), and reduced the overall foam coarsening rate.

Both RC and RCS foams showed similar trends in bubble size growth with oil content. However, their foam half-lives responded differently—RC foam half-life decreased while RCS foam half-life increased—indicating that the coarsening rate was not the critical factor controlling foam half-life in the presence of crude oil. A comparison of RC foam microstructure under oil-free and oil-containing conditions (Fig. S4) revealed that although oil-free foams had thinner films, they were more stable and longer-lasting. This suggests that film stability may play a dominant role in controlling foam half-life under oil-containing conditions.

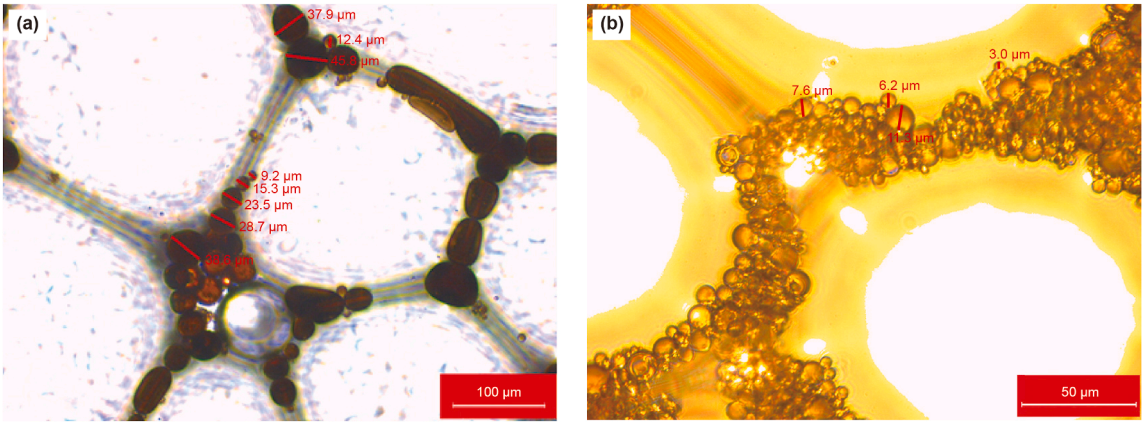

Fig. 11. Microstructure of foams formed by RCS and crude oils with different viscosities after 10 min of foaming at an oil–water ratio of 10%. The oils used were oil C (**a**) and oil E (**b**) and the RCS concentration was 0.2 wt%.

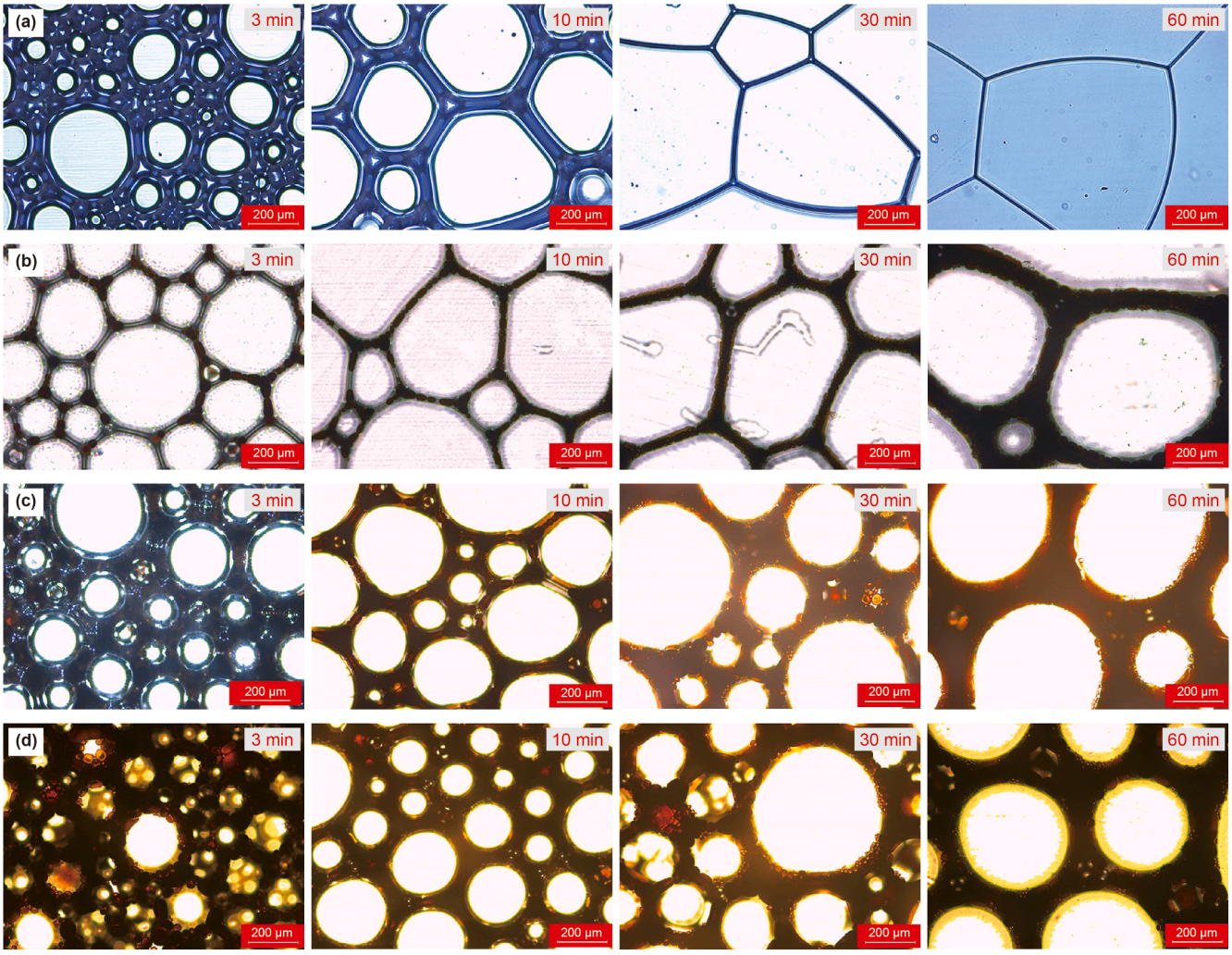

Fig. 12. Microstructure evolution of RCS foam in the presence of oil C. The RCS concentration was 0.2 wt%, with corresponding oil–water ratios of 0 (**a**), 10% (**b**), 40% (**c**), and 60% (**d**), respectively.

3.2.2.2. Pseudoemulsion film stability. Based on Eqs. (1)–(3), surface tension and interfacial tension (IFT) were measured to calculate interaction coefficients between foam systems and crude oils. Table 4 shows that the interaction coefficients for RC and oil C are positive, indicating that oil droplets readily spread on the RC foam film and produce oil bridges between films, leading to foam rupture. In contrast, the interaction coefficients were all negative for RCS when interacting with oils C and E, demonstrating that oil droplets neither entered the film surface nor formed oil bridges.

To validate these interactions, we assessed the stability of pseudoemulsion films under various oil–water ratios. Given that the surfactant concentration in the aqueous phase of the pseudoemulsion film was equivalent to that in the aqueous phase drained from the oil-containing foam, we measured the surfactant concentrations in the drained aqueous phases of RC and RCS oil-containing foams. Table 5 indicates that RCS concentration in the drained aqueous phases decreases with increasing oil–water ratio, with a more pronounced decrease in the presence of oil E. This can be attributed to the formation of smaller emulsified oil droplets with oil E compared to those with oil C, as depicted in Fig. 10, which increased the distribution of RCS at the oil–water interface. Consequently, we conducted stability tests on pseudoemulsion films for foam systems with surfactant concentrations ranging from 0.01 to 0.10 wt%.

Table 6 demonstrates that the stability of the RCS pseudoemulsion film markedly exceeds that of the RC pseudoemulsion film. For the 0.01 wt% RC, oil droplets rapidly entered the gas–water interface and spread on it shortly after the formation of the pseudoemulsion film. In contrast, the pseudoemulsion film formed with 0.01 wt% RCS remained stable for 60 min, matching the stability of the film formed with 0.10 wt% RC. Increasing the RCS concentration to 0.05 wt% enabled the pseudoemulsion films of both crude oils to maintain stability for over 7 d. The stability of pseudoemulsion films increased with foam system concentration, suggesting that higher oil–water ratios corresponded to reduced film stability. This reduction in pseudoemulsion film stability explained the decrease in RC foam half-life with increasing oil–water ratios. However, the increase in RCS foam half-life with oil–water ratio remained an open question.

The negative interaction coefficient between RCS and crude oil, along with the stability of the pseudoemulsion film, suggested that the RCS foam film was resistant to disruption by oil droplets. We speculated that variations in the RCS foam half-life were associated with the intrinsic stability of the RCS foam film. Consequently,

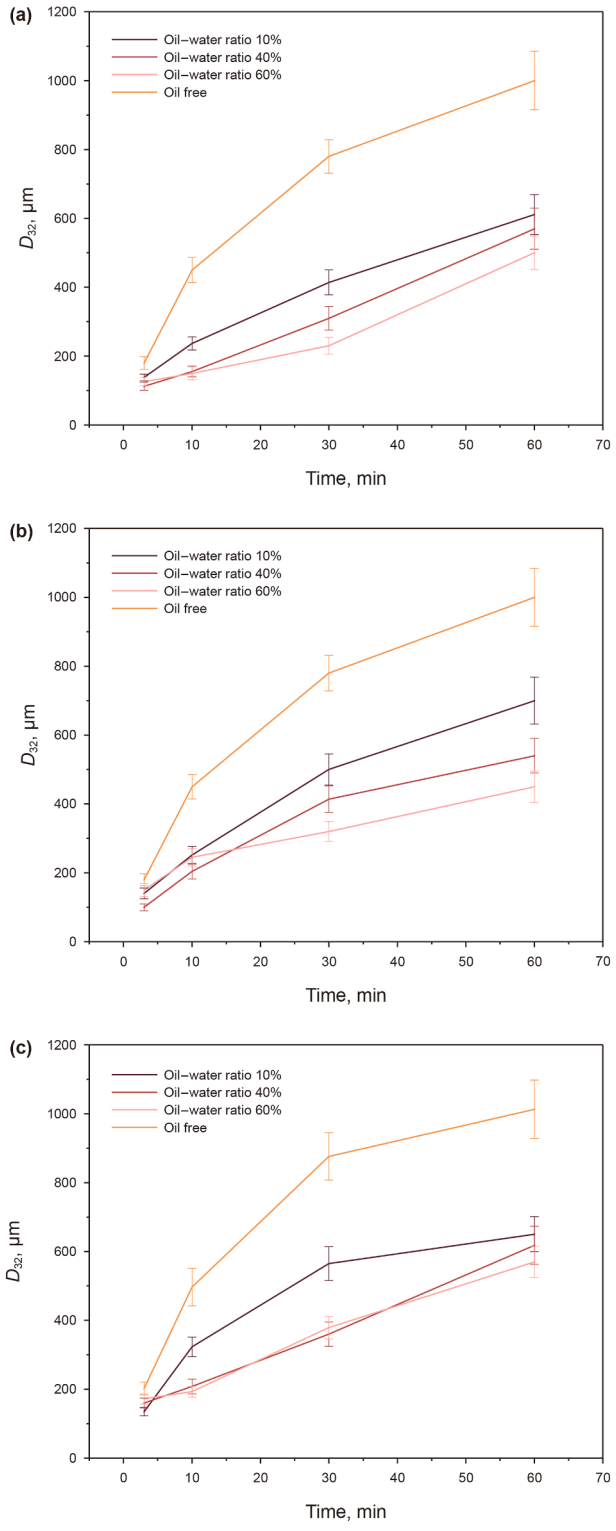

Fig. 13. Mean diameter of bubbles versus time at oil–water ratios of 0, 10%, 40% and 60%. The foam system concentration was 0.2 wt%. RCS foams in the presence of oil C (**a**) and E (**b**); (**c**) RC foam in the presence of oil C.

subsequent investigations focused on the gas–water interface stability of oil-containing foams.

3.2.2.3. Gas–water interface stability of oil-containing foam. Surface dilatational viscoelasticity is a pivotal property of the gas–water interface. A high viscoelastic modulus enables the film to resist disturbances, enhances its strength during thinning, and delays foam coalescence (Wang et al., 2016, 2019). Using the drained water from RCS foam as the aqueous phase, we measured the dilatational viscoelasticity of the gas–water interface under various oil-containing conditions.

Despite the decrease in RCS concentration in the drained aqueous phase relative to the initial system, Fig. 14 indicates that the corresponding surface dilatational viscoelasticity increases. This increase was attributed to the Gibbs–Marangoni effect. At low RCS concentrations, the film's expansion deformation was not sufficiently counteracted by surfactant molecules from the bulk solution to restore the surface tension gradient in the deformed area. As a result, surfactant molecules adjacent to the deformed surface migrated towards it, carrying water molecules to restore the deformed surface, which led to an elevated dilatational modulus and enhanced foam film stability. The enhancement in dilatational viscoelasticity was particularly evident at higher oil–water ratios, consistent with the observed trend in foam half-life as a function of the oil–water ratio. In summary, the stability of the gas–water interface is crucial for the half-life of RCS oil-containing foam with stable pseudoemulsion films.

3.3. Effect of crude oil on steady-state flow characteristics of foam

To evaluate the performance of foam in mobility control, both in the absence and presence of crude oil, we characterized the steady-state flow behavior of foam under different oil-containing conditions.

Fig. 15 illustrates the apparent viscosities of RC and RCS foams in an oil-free environment across various foam qualities. Two distinct regimes were observed based on foam quality f_g: In the low-quality regime, the apparent viscosity increased with foam quality, especially beyond 40%. Ahmed et al. (2017) attributed this to a transition in foam texture from spherical to irregular shapes as the foam quality increased, thereby increasing flow resistance. In the high-quality regime, the apparent viscosity decreased sharply with increasing foam quality due to the elevated capillary pressure. When capillary pressure exceeds the critical value P_c^*, the foam film becomes unstable (Farajzadeh et al., 2015; Adebayo, 2021). The critical foam quality f_g^* for both RC and RCS foams was approximately 80%, but the maximum apparent viscosity of RCS foam was 1.4 times that of RC foam, consistent with its superior bulk foam stability.

Fig. 16 shows the impact of crude oil on the apparent viscosities of RC and RCS foams across various foam qualities. At a 5% oil fractional flow, f_g^* for RC foam decreased to 36%, while that for RCS foam remained constant, suggesting that crude oil was less likely to induce a transition from the low-quality to the high-quality regime in the oil-resistant foam. However, when f_g exceeded 50%, both RC and RCS oil-containing foams showed reduced apparent viscosities compared to oil-free conditions, with reductions of 30.4% and 29.8%, respectively. Hanamertani et al. (2021) reported that foams become more susceptible to crude oil in high-quality regimes. They conducted co-injection tests of foam and crude oil at a f_g of 90% and observed a reduction in apparent viscosity by 37%–48% at an oil fraction of 5%. Furthermore, dry foams, characterized by thinner films and smaller plateau borders in high-quality regimes, facilitate oil entry into the gas–water interface, accelerating film coalescence (Osei-Bonsu et al., 2017).

Hanamertani et al. (2023) and Tang et al. (2019a) also observed that the destabilizing effect of crude oil on foams at high foam qualities becomes more pronounced as the oil fraction increases. To further investigate this behavior, we increased the oil fraction to 10% and assessed the steady-state flow behavior of RCS foam in the

Table 4
Interaction coefficients between foam systems and crude oils.

Foam system	Oil type	Entry coefficient *E*	Spreading coefficient *S*	Bridging coefficient *B*
0.2 wt% RC	Oil C	2.18	1.42	104.20
0.2 wt% RCS	Oil C	−11.35	−12.25	−521.40
0.2 wt% RCS	Oil E	−10.62	−11.98	−493.34

Table 5
Surfactant concentrations in the aqueous phase drained from oil-containing foams.

Foam system	Oil type	Oil–water ratio, %	Surface tension of diluted aqueous phase, mN/m	Surfactant concentration, wt%
RC	Oil C	0	32.90	0.182
		10	35.80	0.137
		40	36.90	0.123
		60	39.50	0.095
RCS	Oil C	0	17.00	0.197
		10	17.15	0.172
		40	22.65	0.102
		60	23.42	0.097
RCS	Oil E	0	17.00	0.179
		10	17.74	0.145
		40	24.00	0.093
		60	27.60	0.072

Table 6
Stability of pseudoemulsion films formed by RC and RCS in the presence of crude oil.

Foam system	Surfactant concentration, wt%	Oil type	Rupture time of pseudoemulsion film
RC	0.01	Oil C	1 min
	0.05		30 min
	0.10		68 min
RCS	0.01	Oil C	60 min
		Oil E	56 min
	0.05	Oil C	> 7 d
		Oil E	> 7 d

presence of crude oil. Despite stable oil-containing foams were observed at the core outlet across a range of foam qualities (Fig. S5), f_g^* for RCS foam decreased to 38%, accompanied by a noticeable reduction in apparent viscosity in the high-quality regime. However, as shown in Table 3, under constant oil fraction, the oil–water ratio increased with foam quality but remained below 60% in all multiphase co-injection experiments. Within this range, the bulk RCS foam exhibited increasing stability. The contrasting behavior between improved bulk foam stability and diminished mobility control in porous media suggests that crude oil has a more adverse effect on foam strength in porous media than in bulk. While bulk foam tests remain a practical and cost-effective tool for initial screening and characterization, they are insufficient for predicting foam performance in porous media. A more comprehensive approach that integrates bulk-phase properties with in-situ flow behavior is essential for accurately evaluating foam behavior under reservoir conditions.

Interestingly, at low foam qualities ($f_g < 50\%$), both RC and RCS foams demonstrated enhanced mobility control in oil-containing environments compared to oil-free conditions. Microstructural examination of the produced fluids revealed that oil E underwent in-situ oil-in-water emulsification when interacting with foam systems. Like foam, emulsions can generate the Jamin effect during flow through porous media, contributing to increased apparent viscosity. For example, when the foam system, N_2, and crude oil were co-injected at $f_o = 5\%$ and $f_g = 20\%$, the apparent viscosities of the RC and RCS systems were 53.0 and 62.1 mPa·s, respectively. In contrast, when the RC and RCS systems were co-injected only with crude oil, their apparent viscosities were 8.2 and 41.6 mPa·s, respectively; when the RC and RCS systems were co-injected only with N_2, the apparent viscosities were 18.4 and 9.2 mPa·s, respectively. These results confirm a synergistic Jamin effect between foam and emulsions, leading to increased flow resistance within the core compared to pure foam or pure emulsions. When f_o was increased to 10%, apparent viscosity at low foam qualities rose sharply, surpassing even the values recorded under oil-free conditions. This suggests that higher oil content, which corresponds to greater emulsion concentration, intensifies the Jamin effect within the porous medium. This observation is consistent with findings reported by Amirmoshiri et al. (2018). Additionally, microscopic analysis of the produced RC and RCS foams after 24 h of static settling ($f_g = 40\%$, $f_o = 5\%$) revealed that the in-situ RCS emulsions consistently maintained an oil-in-water emulsified state, whereas the in-situ RC emulsions experienced phase reversal (see Fig. 17). The ability of RCS to stabilize emulsions in situ may contribute to enhanced foam stability and greater flow resistance in porous media.

Our experiments demonstrated a clear correlation between the mobility control capability of foam and its emulsification behavior in oil-containing environments. However, the relationship between oil saturation and the flow resistance of foam–emulsion mixtures was not directly quantified in this study. Based on the observed mechanisms, it is reasonable to expect that in low-permeability, oil-rich regions, the amplified Jamin effect could raise local resistance to a level that destabilizes the displacement front. Conversely, the same mechanism could be

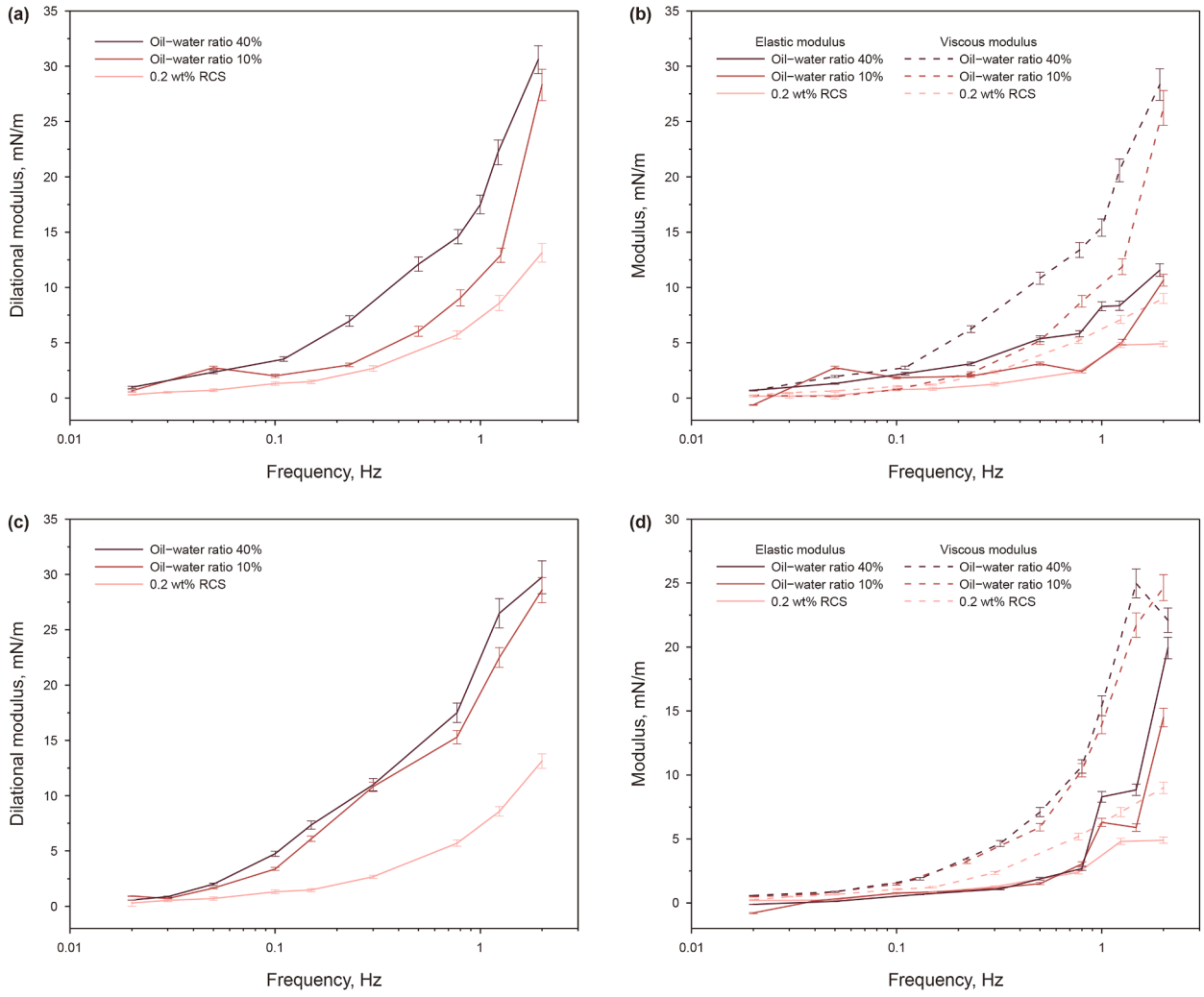

Fig. 14. Surface dilatational viscoelasticity of the aqueous phase drained from RCS foam at different oil–water ratios. The foam system concentration was 0.2 wt%. Dilatational modulus (**a**) and elastic and viscous moduli (**b**) in the presence of oil C. Dilatational modulus (**c**) and elastic and viscous moduli (**d**) in the presence of oil E.

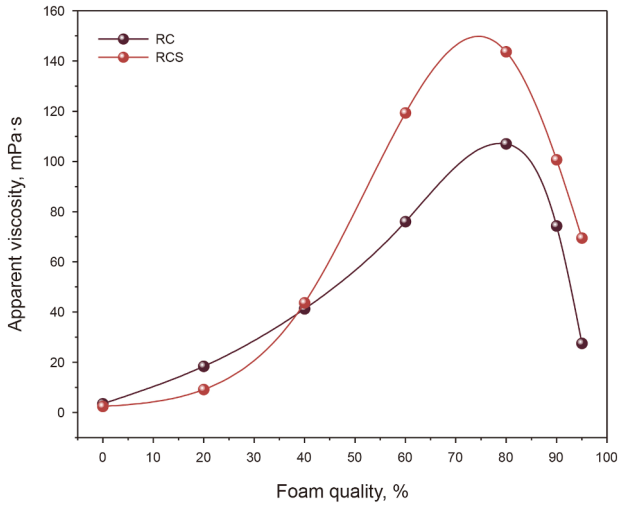

Fig. 15. Apparent viscosities of RC and RCS foams under different foam qualities without oil. The foam system concentration was 0.2 wt%.

advantageous in high-permeability thief zones, where increased resistance may enhance sweep efficiency. The net outcome is therefore contingent on the spatial distribution of oil saturation and the local foam–emulsion flow behavior. These interactions warrant careful consideration in the design of injection strategies and in the accurate prediction of foam performance in EOR applications.

3.4. Limitations

Several limitations of this study should be acknowledged. First, bulk foam and interfacial property measurements were conducted at 25 °C and atmospheric pressure to isolate fundamental stability mechanisms under controlled conditions. While the observed trends were consistent with separate HTHP coreflood tests, no bulk HTHP experiments were performed. As such, the ambient-condition results should be considered qualitative indicators of reservoir-relevant behavior rather than quantitative predictors. Second, although key factors, such as surfactant concentration and crude oil type/content, were controlled, other influential parameters were not tightly quantified. These included the initial bubble

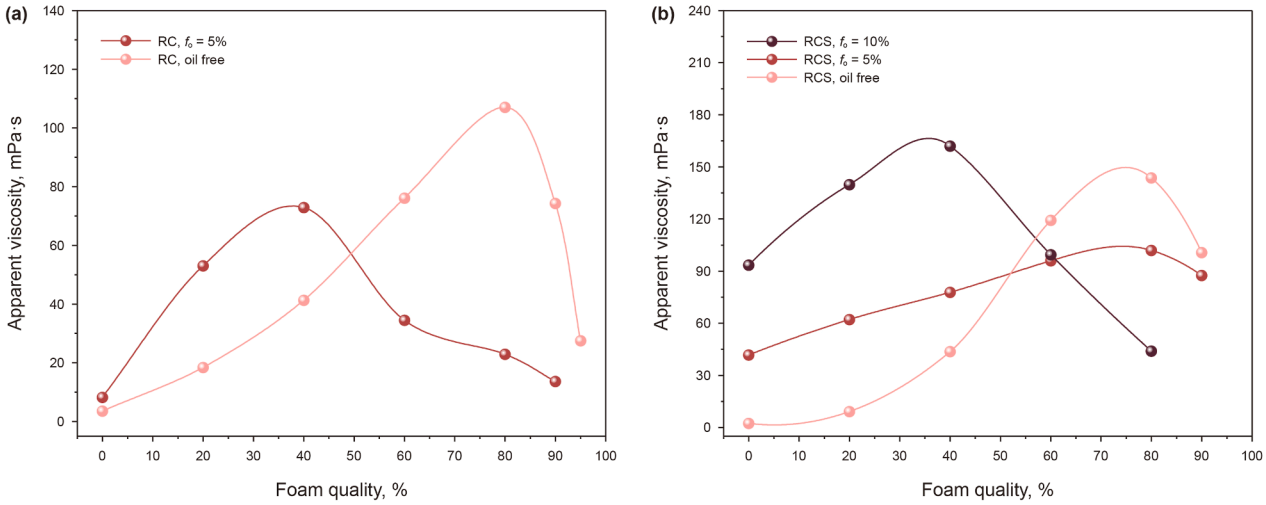

Fig. 16. Apparent viscosities of RC (**a**) and RCS (**b**) foams under different foam qualities in the presence of oil E. The foam system concentration was 0.2 wt%.

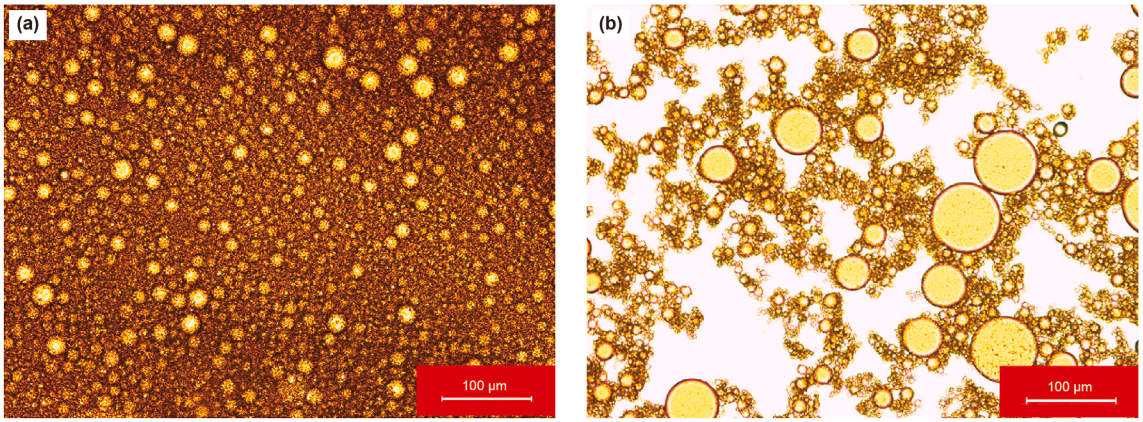

Fig. 17. Microscopic images of drained liquids after 24 h of static settling for RC (**a**) and RCS (**b**) foams. The foam system concentration was 0.2 wt%, the oil used was oil E, the foam quality was 40%, and the crude oil fractional flow was 5%.

size distribution and subtle variations in foam generation history. Such factors could contribute to deviations between the measured data and the true system behavior, even though triplicate testing was used to reduce random error.

4. Conclusions

This study comprehensively examined the properties of bulk foams in the presence of crude oil and the co-permeation behavior of the crude oil–N_2–foam system under high-salinity conditions. The key findings are summarized as follows.

(1) The foam system RC, composed of an anionic-nonionic surfactant and a betaine surfactant, produced foams with a longer drainage half-life but a shorter foam half-life in the presence of high-viscosity oil ($\geq$ 650 mPa·s) compared to oil-free conditions. Introducing the oil-resistant additive OS into the RC at a 3:7 mass ratio formulated the foam system RCS, which significantly improved foam film tolerance to crude oil, especially for oils with low to medium viscosities (10.8–650 mPa·s).

(2) The RCS emulsified crude oil into stable droplets, with droplet size positively related to oil viscosity. For high-viscosity oil, larger droplets formed and aggregated within theplateau borders, reducing drainage channels and extending drainage half-life as the oil–water ratio increased up to 60%. For low-viscosity oils, smaller droplets drained more readily than water, leading to a decrease in drainage half-life beyond an oil–water ratio of 10%.

(3) For RC oil-containing foam, foam half-life was primarily controlled by pseudoemulsion film stability. As the oil–water ratio increased, the surfactant concentration within the film decreased, weakening its structure and reducing the foam half-life. In contrast, RCS oil-containing foams featured highly stable pseudoemulsion films, with half-life instead governed by the stability of the gas–water interface. In this case, increasing the oil–water ratio enhanced the dilatational viscoelasticity of the gas–water interface, thereby prolonging the foam half-life.

(4) Under oil-free conditions, optimal mobility control for both RC and RCS foams was achieved at foam qualities near 80%. The presence of crude oil reduced foam strength in porous

media and shifted f_g^* to lower values. RCS foam, with superior oil resistance, exhibited this shift at higher oil fractional flows than RC foam.

(5) At low foam quality (f_g < 50%), in-situ emulsification enhanced the flow resistance of RCS foam. The combined action of foam and emulsions generated a synergistic effect, offering a promising approach for enhancing mobility control in oil-containing porous media.

CRediT authorship contribution statement

Lin Sun: Writing – review & editing, Funding acquisition, Conceptualization. **Jia-Qi Yin:** Investigation. **Hong-Ying Sun:** Writing – original draft, Investigation. **Yan-Ping Wu:** Writing – original draft, Investigation. **Wan-Fen Pu:** Conceptualization. **Bing Wei:** Writing – review & editing, Conceptualization.

Declaration of competing interest

The authors declare that they have no known competing financial interests or personal relationships that could have appeared to influence the work reported in this paper.

Acknowledgements

The authors gratefully acknowledge the financial support of National Natural Science Foundation of China (52474049), Oil & Gas Major Project (2025ZD1407202), Natural Science Foundation of Sichuan Province (2024NSFSC0198), and the Tianfu Yongxing Laboratory Organized Research Project Funding (2023KJGG17).

Appendix A. Supplementary data

Supplementary data to this article can be found online at https://doi.org/10.1016/j.petsci.2025.11.014.

References

Adebayo, A.R., 2021. Foam flow in different pore systems—Part 2: The roles of pore attributes on the limiting capillary pressure, trapping coefficient, and relative permeability of foamed gas. SPE J. 26 (6), 3926–3948. https://doi.org/10.2118/205523-PA.

Ahmadi, H.A., Ebadi, A., Hosseinalipour, S.M., 2023. Experimental study of bubble-droplet interaction in water; the effect of water salinity on the drainage time. J. Dispersion Sci. Technol. 44 (1), 61–74. https://doi.org/10.1080/01932691.2021.1930037.

Ahmed, S., Elraies, K.A., Hashmet, M.R., Shaifan, S.R.B.M., Hsia, I.C., Bahrim, R.Z., 2017. Experimental investigation and optimization of polymer enhanced CO_2 foam stability and apparent viscosity. In: SPE Kingdom of Saudi Arabia Annual Technical Symposium and Exhibition. https://doi.org/10.2118/188018-MS.

Amani, P., Miller, R., Ata, S., Hurter, S., Rudolph, V., Firouzi, M., 2020. Dynamics of interfacial layers for sodium dodecylbenzene sulfonate solutions at different salinities. J. Ind. Eng. Chem. 92, 174–183. https://doi.org/10.1016/j.jiec.2020.09.002.

Amirmoshiri, M., Zeng, Y., Chen, Z., Singer, P.M., Puerto, M.C., Grier, H., Bahrim, R.Z.K., Vincent-Bonnieu, S., Farajzadeh, R., Biswal, S.L., Hirasaki, G.J., 2018. Probing the effect of oil type and saturation on foam flow in porous media: Core-flooding and nuclear magnetic resonance (NMR) imaging. Energy & Fuels 32 (11), 11177–11189. https://doi.org/10.1021/acs.energyfuels.8b02157.

Amirmoshiri, M., Wang, X., Bai, C., Tewari, R.D., Xie, S.X., Bahrim, R.Z.K., Singer, P.M., Farajzadeh, R., Biswal, S.L., Hirasaki, G.L., 2021. Distinguishing the effect of rock wettability from residual oil on foam generation and propagation in porous media. Energy & Fuels 35 (9), 7681–7692. https://doi.org/10.1021/acs.energyfuels.0c04247.

Andrianov, A., Farajzadeh, R., Nick, M.M., Talanana, M., Pacelli, L.Z., 2011. Immiscible foam for enhancing oil recovery: Bulk and porous media experiments. In: SPE Enhanced Oil Recovery Conference. https://doi.org/10.2118/143578-MS.

Aveyard, R., Binks, B.P., Fletcher, P.D.I., Peck, T.G., Rutherford, C.E., 1994. Aspects of aqueous foam stability in the presence of hydrocarbon oils and solid particles. Adv. Colloid. Interface. 48, 93–120. https://doi.org/10.1016/0001-8686(94)80005-7.

Babamahmoudi, S., Riahi, S., 2018. Application of nano particle for enhancement of foam stability in the presence of crude oil: Experimental investigation. J. Mol. Liq. 264, 499–509. https://doi.org/10.1016/j.molliq.2018.04.093.

Etemad, S., Kantzas, A., Bryant, S., 2020. Efficient nanoparticle transport via CO_2 foam to stabilize oil in water emulsions. Fuel 276, 118063. https://doi.org/10.1016/j.fuel.2020.118063.

Farajzadeh, R., Andrianov, A., Krastev, R., Hirasaki, G.J., Rossen, W.R., 2012. Foam–oil interaction in porous media: Implications for foam assisted enhanced oil recovery. Adv. Colloid. Interface. 183–184, 1–13. https://doi.org/10.1016/j.cis.2012.07.002.

Farajzadeh, R., Lotfollahi, M., Eftekhari, A.A., Rossen, W.R., Hirasaki, G.J.H., 2015. Effect of permeability on implicit-texture foam model parameters and the limiting capillary pressure. Energy & Fuels 29 (5), 3011–3018. https://doi.org/10.1021/acs.energyfuels.5b00248.

Garrett, P.R., 1980. Preliminary considerations concerning the stability of a liquid heterogeneity in a plane-parallel liquid film. J. Colloid Interface Sci. 76 (2), 587–590. https://doi.org/10.1016/0021-9797(80)90400-2.

Guo, H., Lyu, X., Meng, E., Xu, Y., Zhang, M., Fu, H., Zhang, Y., Song, K., 2022. CCUS in China: Challenges and opportunities. In: SPE Improved Oil Recovery Conference. https://doi.org/10.2118/209468-MS.

Hanamertani, A.S., Saraji, S., Piri, M., 2021. The effects of in-situ emulsion formation and superficial velocity on foam performance in high-permeability porous media. Fuel 306, 121575. https://doi.org/10.1016/j.fuel.2021.121575.

Hanamertani, A.S., Saraji, S., Piri, M., 2023. A comparative investigation of the effect of gas type on foam strength and flow behavior in tight carbonates. Chem. Eng. Sci. 276, 118798. https://doi.org/10.1016/j.ces.2023.118798.

Harati, S., Bayat, A.E., Sarvestani, M.T., 2020. Assessing the effects of different gas types on stability of SiO_2 nanoparticle foam for enhanced oil recovery purpose. J. Mol. Liq. 313, 113521. https://doi.org/10.1016/j.molliq.2020.113521.

Harkins, W.D., 1941. A general thermodynamic theory of the spreading of liquids to form duplex films and of liquids or solids to form monolayers. J. Chem. Phys. 9 (7), 552–568. https://doi.org/10.1063/1.1750953.

Harkins, W.D., Feldman, A., 1922. Films. The spreading of liquids and the spreading coefficient. J. Am. Chem. Soc. 44 (12), 2665–2685. https://doi.org/10.1021/ja01433a001.

Hassan, A.M., Ayoub, M., Eissa, M., Bruining, H., Zitha, P., 2020. Study of surface complexation modeling on a novel hybrid enhanced oil recovery (EOR) method; smart-water assisted foam-flooding. J. Petrol. Sci. Eng. 195, 107563. https://doi.org/10.1016/j.petrol.2020.107563.

He, G., Li, H., Guo, C., Liao, J., Deng, J., Liu, S., Dong, H., 2022. Stable foam systems for improving oil recovery under high-temperature and high-salt reservoir conditions. J. Petrol. Sci. Eng. 211, 110145. https://doi.org/10.1016/j.petrol.2022.110145.

Jamaloei, B.Y., Kharrat, R., 2012. The lessons learned from miscible gas flooding in naturally fractured reservoirs: Integrated studies, and pilot and field cases. Petrol. Sci. Technol. 30 (17), 1802–1812. https://doi.org/10.1080/10916466.2010.511388.

Kim, J.S., Dong, Y., Rossen, W.R., 2004. Steady-state flow behavior of CO_2 foam. In: SPE/DOE Symposium on Improved Oil Recovery. https://doi.org/10.2118/89351-MS.

Koczo, K., Lobo, L.A., Wasan, D.T., 1992. Effect of oil on foam stability: Aqueous foams stabilized by emulsions. J. Colloid Interface Sci. 150 (2), 492–506. https://doi.org/10.1016/0021-9797(92)90218-B.

Lai, N., Zhao, J., Zhu, Y., Wen, Y., Huang, Y., Han, J., 2021. Influence of different oil types on the stability and oil displacement performance of gel foams. Colloids Surf. 630, 127674. https://doi.org/10.1016/j.colsurfa.2021.127674.

Lee, J., Nikolov, A., Wasan, D., 2014. Surfactant micelles containing solubilized oil decrease foam film thickness stability. J. Colloid Interface Sci. 415, 18–25. https://doi.org/10.1016/j.jcis.2013.10.014.

Li, B.F., Zhang, M.Y., Li, Z.M., Kovscek, A., Yan, X., Li, B.L., 2023. Flow characteristics and regime transition of aqueous foams in porous media over a wide range of quality, velocity, and surfactant concentration. Pet. Sci. 20 (2), 1044–1052. https://doi.org/10.1016/j.petsci.2022.11.014.

Liang, S., Hu, S., Li, J., Xu, G., Zhang, B., Zhao, Y., Yan, H., Li, J., 2019. Study on EOR method in offshore oilfield: Combination of polymer microspheres flooding and nitrogen foam flooding. J. Petrol. Sci. Eng. 178, 629–639. https://doi.org/10.1016/j.petrol.2019.03.078.

Ma, K., Liontas, R., Conn, C.A., Hirasaki, G.J., Biswal, S.L., 2012. Visualization of improved sweep with foam in heterogeneous porous media using microfluidics. Soft Matter 8 (41), 10669–10675. https://doi.org/10.1039/C2SM25833A.

Majeed, T., Sølling, T.I., Kamal, M.S., 2020. Foamstability: The interplay between salt-, surfactant- and critical micelle concentration. J. Petrol. Sci. Eng. 187, 106871. https://doi.org/10.1016/j.petrol.2019.106871.

Mensire, R., Lorenceau, E., 2017. Stable oil-laden foams: Formation and evolution. Adv. Colloid. Interface. 247, 465–476. https://doi.org/10.1016/j.cis.2017.07.027.

Moradpour, N., Yang, J., Tsai, P.A., 2024. Liquid foam: Fundamentals, rheology, and applications of foam displacement in porous structures. Curr. Opin. Colloid. 74, 101845. https://doi.org/10.1016/j.cocis.2024.101845.

Osei-Bonsu, K., Grassia, P., Shokri, N., 2017. Investigation of foam flow in a 3D printed porous medium in the presence of oil. J. Colloid Interface Sci. 490, 850–858. https://doi.org/10.1016/j.jcis.2016.12.015.

Osterloh, W.T., Jante, M.J., 1992. Effects of gas and liquid velocity on steady-state foam flow at high temperature. In: SPE/DOE Enhanced Oil Recovery Symposium. https://doi.org/10.2118/24179-MS.

Pu, W., Pang, S., Wang, C., 2017. Experimental investigation of foam performance in the presence of crude oil. J. Surfactants Deterg. 20 (5), 1051–1059. https://doi.org/10.1007/s11743-017-1991-3.
Pu, W., Wei, P., Sun, L., Pu, Y., Chen, Y., 2019. Investigation on stabilization of foam in the presence of crude oil for improved oil recovery. J. Dispersion Sci. Technol. 40 (5), 646–656. https://doi.org/10.1080/01932691.2018.1476153.
Ritacco, H.A., 2024. Foam-assisted oil recovery: A physics-based perspective. Curr. Opin. Colloid. In. 72, 101809. https://doi.org/10.1016/j.cocis.2024.101809.
Rohani, M.R., Ghotbi, C., Badakhshan, A., 2014. Foam stability and foam-oil interactions. Petrol. Sci. Technol. 32 (15), 1843–1850. https://doi.org/10.1080/10916466.2012.683920.
Roncoroni, M.A., Romero, P., Montes, J., Bascialla, G., Rodríguez, R., Pons-Esparver, R.R., Mazadiego, L.F., García-Mayoral, M.F., 2021. Enhancement of a foaming formulation with a zwitterionic surfactant for gas mobility control in harsh reservoir conditions. Pet. Sci. 18 (5), 1409–1426. https://doi.org/10.1016/j.petsci.2021.08.004.
Simjoo, M., Zitha, P.L., 2013. Effects of oil on foam generation and propagation in porous media. In: SPE Enhanced Oil Recovery Conference. https://doi.org/10.2118/165271-MS.
Stein, M.H., Frey, D.D., Walker, R.D., Pariani, G.J., 1992. Slaughter estate unit co_2 flood: Comparison between pilot and field-scale performance. J. Petrol. Technol. 44 (9), 1026–1032. https://doi.org/10.2118/19375-PA.
Sun, L., Wei, P., Pu, W., Wang, B., Wu, Y., Tan, T., 2016. The oil recovery enhancement by nitrogen foam in high-temperature and high-salinity environments. J. Petrol. Sci. Eng. 147, 485–494. https://doi.org/10.1016/j.petrol.2016.09.023.
Sun, L., Bai, B., Wei, B., Pu, W., Wei, P., Li, D., Zhang, Y., 2019. Recent advances of surfactant-stabilized N_2/CO_2 foams in enhanced oil recovery. Fuel 241, 83–93. https://doi.org/10.1016/j.fuel.2018.12.016.
Sun, L., Chen, D., Zhang, Y., Sun, X., Pu, W., Wei, B., Tang, J., Sun, X., 2022. Probing high-salinity-enhanced stability of betaine foam for foam application in harsh reservoirs. Fuel 327, 125144. https://doi.org/10.1016/j.fuel.2022.125144.
Sun, L., Sun, X.H., Zhang, Y.C., Xin, J., Sun, H.Y., Li, Y.B., Pu, W.F., Tang, J.Y., Wei, B., 2023. Stability of high-salinity-enhanced foam: Surface behavior and thin-film drainage. Pet. Sci. 20 (4), 2343–2353. https://doi.org/10.1016/j.petsci.2023.01.012.
Talebian, S.H., Masoudi, R., Tan, I.M., Zitha, P.L.J., 2014. Foam assisted CO_2-EOR: A review of concept, challenges, and future prospects. J. Petrol. Sci. Eng. 120, 202–215. https://doi.org/10.1016/j.petrol.2014.05.013.
Tang, J., Vincent-Bonnieu, S., Rossen, W.R., 2019a. Experimental investigation of the effect of oil on steady-state foam flow in porous media. SPE J. 24 (1), 140–157. https://doi.org/10.2118/194015-PA.
Tang, J., Ansari, M.N., Rossen, W.R., 2019b. Quantitative modeling of the effect of oil on foam for enhanced oil recovery. SPE J. 24 (3), 1057–1075. https://doi.org/10.2118/194020-PA.
Tang, X.C., Li, Y.Q., Liu, Z.Y., Zhang, N., 2023. Nanoparticle-reinforced foam system for enhanced oil recovery (EOR): Mechanistic review and perspective. Pet. Sci. 20 (4), 2282–2304. https://doi.org/10.1016/j.petsci.2022.12.007.
Telmadarreie, A., Trivedi, J.J., 2018. Static and dynamic performance of wet foam and polymer-enhanced foam in the presence of heavy oil. Colloid. Interface. 2 (3), 38. https://doi.org/10.3390/colloids2030038.
Vikingstad, A.K., Skauge, A., Høiland, H., Aarra, M., 2005. Foam–oil interactions analyzed by static foam tests. Colloids Surf., A 260 (1), 189–198. https://doi.org/10.1016/j.colsurfa.2005.02.034.
Wang, G., Dong, P., Lu, Y., Zeng, M., Zhang, Q., 2021. Experimental and theoretical investigation on the surface tension of nano-lithium bromide solution. Int. Commun. Heat. Mass. 123, 105231. https://doi.org/10.1016/j.icheatmasstransfer.2021.105231.
Wang, H., Wei, X., Du, Y., Wang, D., 2019. Experimental investigation on the dilatational interfacial rheology of dust-suppressing foam and its effect on foam performance. Process. Saf. Environ. 123, 351–357. https://doi.org/10.1016/j.psep.2019.01.027.
Wang, J., Nguyen, A.V., Farrokhpay, S., 2016. Effects of surface rheology and surface potential on foam stability. Colloids Surf., A 488, 70–81. https://doi.org/10.1016/j.colsurfa.2015.10.016.
Wei, P., Pu, W., Sun, L., Pu, Y., Wang, S., Fang, Z., 2018. Oil recovery enhancement in low permeable and severe heterogeneous oil reservoirs via gas and foam flooding. J. Petrol. Sci. Eng. 163, 340–348. https://doi.org/10.1016/j.petrol.2018.01.011.
Wei, P., Guo, K., Xie, Y., 2020. Polysaccharide-stabilized oil-laden foam for enhancing oil recovery. J. Pet. Sci. Eng. 195, 107597. https://doi.org/10.1016/j.petrol.2020.107597.
Won, J.Y., Krägel, J., Makievski, A.V., Gochev, G., Loglio, G., Pandolfini, P., Leser, M.E., Gehin-Delval, C., Miller, R., 2014. Drop and bubble micro manipulator (DBMM)—A unique tool for mimicking processes in foams and emulsions. Colloids Surf., A 441, 807–814. https://doi.org/10.1016/j.colsurfa.2013.04.027.
Yan, W., Miller, C.A., Hirasaki, G.J., 2006. Foam sweep in fractures for enhanced oil recovery. Colloids Surf., A 282–283, 348–359. https://doi.org/10.1016/j.colsurfa.2006.02.067.